Sub-Line Transient Magnetic Fields Calculation Approach for Fault detection, classification and location of High Voltage Transmission Line

Abdelrahman Said Ghoniem

Electrical power and machine department, Faculty of Engineering at Shoubra, Benha University, Cairo, Egypt
abdelrahman.ghoniem@feng.bu.edu.eg, abdo_eng1987@yahoo.com

Abstract: This paper uses ATP/EMTP to simulate different fault types as single line to ground fault, three phases to ground fault, double line fault, direct lightning strokes, and flashover for Egyptian Bassous-Cairo West 500 kV transmission line single circuit. By using 3D Biot-Savart Law technique, the measured current at sending end using substation optic fiber CT utilized for calculating transient magnetic field, and then certain comparing of selected features of the calculated transient magnetic field under different phases are used for fault detection and classification. The results show that the calculated transient magnetic field at sending end have unique shape for each abnormal condition, so it is very effective to extract the transient components from the fault signals, then detection and classification of faults can be done accurately. The fault location scheme is based on divide line length into sections each section contain only one sensor, then the comparison between measured transient magnetic field from installed non contact, 3-axis Magnetoresistance, magnetic field sensors at tower section sensors and calculated measured transient magnetic field from substation optic fiber CT. It was discovered that this method is able to offer high accuracy fault location.

Keywords: Faults, Fault location, Transient magnetic field, ATP-EMTP, Biot-Savart Law, CT, Lightning strokes, Magnetoresistance sensor.

1. Introduction

Transmission lines are exposed to temporary and permanent faults. Temporary faults are mostly self cleared and permanent faults can be detected and mitigated with the help of traditionally available protective relay equipments [1- 3].

Many faults in overhead power lines are transient in nature and power system protection devices operate to isolate the area of the fault, clear the fault and then the power-line can be returned to service.

In practice, most faults in power systems are unbalanced. However, asymmetric faults are difficult to analyze. The common types of asymmetric faults are single phase to ground fault, line to line fault, double line to ground fault [4].

Statistics show that line faults are the most common fault in power systems [3]. So it is very important to detect it and to find its location in order to take necessary remedial actions and to restore power as soon as possible.

Over the years, much research has been done on the various techniques for accurate fault location detection. Many methods use line data from one or more terminals for determining the fault locations and they can be categorized as analytical methods, artificial intelligence (AI) based methods, travelling wave methods and software based methods [5-13].

These methods produce reasonable fault location results. However, all these methods based on the available voltage and current measurements across the terminals of the faulted lines by connected devices. For example, in traveling-wave-based approach, the accuracy of the location is highly dependent on the performance of the costly high-speed data acquisition system and the fault location is determined by timing analysis of the travelling wave. In impedance-measurement based technique, the voltage and current during pre-fault and post-fault are acquired and analyzed. The line parameters can then be calculated with the transmission line model and the fault can be located [10].

Furthermore, these methods fully depend on an assumption that the parameters of the transmission line are uniform [11].

In this paper, the transient faults, direct lightning strokes and flashover in Egyptian Bassous-Cairo West 500-kV transmission line single circuit are analyzed. Bassous-Cairo West power line under study have length 7500 m, transmitted power is 500 MVA, 400 m span, 3.307+ j14.053 positive & negative sequence impedance per phase in Ω, two ground wire each has 11.2 mm diameter, three sub-conductor in each phase has 30.6 mm diameter, and its maximum flowing current is 940 A and its voltage is 500 kV.

The magnetic fields are determined under normal and abnormal conditions by using 3d technique, Biot-Savart Law, Furthermore, detection and determination the location of various types of transient on a transmission line introduced.

This paper introduces new method, which only measured current under different conditions from optic fiber CT placed at substation entrance, sending end. Then the data are transmitted to a data-processing center where Matlab software analysis, where the transient magnetic field from each line and resultant field under normal operation and abnormal operation were calculated. The final step, accurate fault classification detection obtained by comparing different lines transient magnetic fields ratio in each condition.

This method considered a low-cost high-precision solution, only sending end CT used for fault detection and classification.

It's clear that the high ratio of resultant transient magnetic field (Bt measured at tower using sensor/ Bt calculated at sending end using CT), indicate fault location section. Different faults and locations are simulated by ATP/EMTP [14], and then certain selected features of the calculated transient magnetic field were analyzed using Matlab software.

2. Modeling and Simulation of the Power Line

ATP-EMTP is used to simulate a high voltage 500 kV Bassous-Cairo west power line under normal and different abnormal conditions.

Including gantry total nineteen towers, 500 kV single circuits with two overhead ground wire, are represented in the simulation model. The phase conductor and ground wire are explicitly modelled between the towers; Figure 1 shows the span of eighteen towers (M1 to M18) between Cairo west/bassous substations.
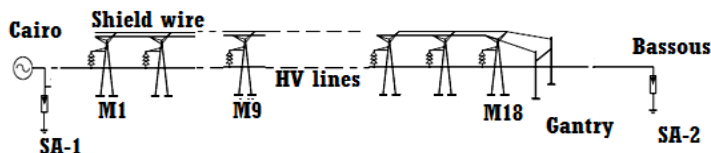

Figure 1. Model of 500 kV line

By assuming each tower has four legs connected in parallel; each leg is grounded with a vertical rod, the rod has a length of (1.5 m) with radius of (1.25 cm), the spacing between these rods is large and enough to neglect the interaction between them and the mutual impedance between horizontal grounding conductors and vertical rods is not considered. The soil parameters such as ρ are taken as 100 Ω.m, εr and μr are taken as 10 and 1, respectively [15, 16]. The nonlinear behaviour of the ground resistance of the rod is considered to get an accurate performance of the grounding rod.

The ground resistance is calculated based on the following equation [14]. Where R (t) in Ω and given by:

$$R(t) = \begin{cases} R_0 = \dfrac{\rho}{2\pi l}\{\ln\dfrac{4l}{a}-1\} \rightarrow For(i < \dfrac{E_0 * \rho}{2\pi R_0^2}) \\[4mm] \dfrac{R_0}{\sqrt{1+\dfrac{i}{\dfrac{E_0 * \rho}{2\pi R_0^2}}}} \rightarrow For(i \geq \dfrac{E_0 * \rho}{2\pi R_0^2}) \end{cases} \quad (1)$$

where, i is the current through the rod (kA), E_0 is the critical soil ionization gradient (in this study is taken as 300 kV/m as a case study). The constant resistance R_o (Ω) of the model is based on the rod dimensions and the soil parameters [16]:

Single three phase circuit is carried on its steel tower, as shown in figure 2. Each phase contains three sub-conductors, which are fixed by right angle.

The simulation of the overhead transmission lines carried out using LCC JMarti model (Frequency dependent model with constant transformation matrix) also based on travelling wave theory [17].

Figure 2 shows the main tower type and geometry used in this study. Leg and cross arms can be modeled with its equivalent surge impedances and propagation velocity. The surge impedance for each part of tower is 200 Ω and the propagation velocity is 2.5 *10^8 m/s [18]. The surge impedance of the gantry is 104Ω [17, 18].

A 500 kV line insulator string modelled as a linear resistor R and capacitor C connected in parallel, having a total equivalent capacitance of 3.94 pF [16] and equivalent resistance 4421 MΩ [16, 17].

Flashover voltage (V_{fo}) is calculated from Eq. (2) depending on elapsed time (t).

$$V_{fo} = (400 + \frac{710}{t^{0.75}}) * L$$

(2)

where, V_{fo} is flashover voltage, kV, L is the insulator string length, m, and t is elapsed time after lightning stroke in µs.

In this paper the selected Pinceti and giannettoni surge arrester 318 kV/rms (MCOV) of arresters with L_1 and L_0 equal 21.75µH, and 0.29 µH [16, 17, 19].
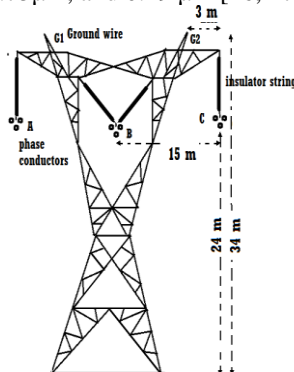

Figure 2. Typical configuration of 500 kV transmission tower

3. Magnetic Field Calculations

In this section the magnetic field generated by sagging overhead conductors including ground wires is deduced. To evaluate impact of magnetic field on catenary (Sagged conductor) suspended between two transmission tower; Consider, (x_i, y_i, z_i) being the coordinates of the conductor and L the distance between two adjacent towers (span) and magnetic field ($d\vec{B}_i$) generated by a small cross sectional length ($d\vec{L}_i$) at distance ($\vec{r}$) when current(I) flows through phase conductor (i). The magnetic field produced by a multiphase conductors (n), and their images, in support structures at any sensing field point (x,y,z) shown in figure. 3 can be obtained by using the Biot-Savart law, 3-D Technique, as follow [20-21, 34]:

$$d\vec{B}_i = \frac{\mu_0 I_i}{4\pi} * \frac{d\vec{L}_i \times \vec{r}}{|\vec{r}|^3}$$

(3)

The equations of the catenary shape of conductor i placed in the y-z plane is given by,

$$d\vec{l}_i = dy_i \vec{a}_y + dz_i \vec{a}_z = \sinh\left(\frac{z_i}{a}\right) dz_i \vec{a}_y + dz_i \vec{a}_z$$

(4)

$$y_i = a\cosh\left(\frac{z_i}{a}\right) + h_i - a \tag{5}$$

where (h_i) the lowest height of the ith conductor above the ground (height at mid-span), $\mu_0 = 4\pi*10^{\wedge}-7\left(N/A^2\right)$ permeability of free space, and (a) parameter associated with the mechanical parameters of the line, a = T_h / w, where T_h is the conductor tension at mid-span and w is the weight per-unit length of the line.

The magnetic field caused by the image currents must be considered. The complex depth ζ of each conductor's image current can be found as given in [22].

$$\zeta = \sqrt{2}\delta e^{-i\frac{\pi}{4}} \tag{6}$$

$$\delta = 503\sqrt{\frac{\rho g}{f}} \tag{7}$$

where: δ is the skin depth of the earth, ρ is the resistivity of the earth, and f is the frequency of the source current in Hz

By applying the Biot Savart law described in Eq. (3), the magnetic field generated by a sagging conductor in any point is given by eqs.(8-10)[23-25],

$$B_{i,x} = \frac{\mu_0 I_i}{4\pi}^{\wp} \int_{-L/2}^{L/2} \left[\frac{\sinh(z_i/a)(z-z_i)-(y-y_i)}{[(x-x_i)^2+(y-y_i)^2+(z-z_i)^2]^{3/2}} - \frac{\sinh(z_i/a)(z-z_i)-(y+y_i+2\zeta)}{[(x-x_i)^2+(y+y_i+2\zeta)^2+(z-z_i)^2]^{3/2}}\right]dz_i \tag{8}$$

$$B_{i,y} = \frac{\mu_0 I_i}{4\pi}^{\wp} \int_{-L/2}^{L/2} \left(\frac{(x-x_i)}{[(x-x_i)^2+(y-y_i)^2+(z-z_i)^2]^{3/2}} - \frac{(x-x_i)}{[(x-x_i)^2+(y+y_i+2\zeta)^2+(z-z_i)^2]^{3/2}}\right)dz_i \tag{9}$$

$$B_{i,z} = \frac{\mu_0 I_i}{4\pi}^{\wp} \int_{-L/2}^{L/2} \left(\frac{-\sinh(z_i/a)(x-x_i)}{[(x-x_i)^2+(y-y_i)^2+(z-z_i)^2]^{3/2}} + \frac{-\sinh(z_i/a)(x-x_i)}{[(x-x_i)^2+(y+y_i+2\zeta)^2+(z-z_i)^2]^{3/2}}\right)dz_i \tag{10}$$

Power lines generally consist of several phase conductors and shield wires. By superposition [23-25, 34], the magnetic field of a transmission line can be written by adding the field components given by Eqs. (8), (9) and (10) for each conductor. The total resultant fields for n conductors are:

$$(Phase(A))B_a = B_{x_a}.\vec{a}_x + B_{y_a}.\vec{a}_y + B_{z_a}.\vec{a}_z \tag{11}$$

$$(Phase(B))B_b = B_{x_b}.\vec{a}_x + B_{y_b}.\vec{a}_y + B_{z_b}.\vec{a}_z \tag{12}$$

$$(Phase(C))B_c = B_{x_c}.\vec{a}_x + B_{y_c}.\vec{a}_y + B_{z_c}.\vec{a}_z \tag{13}$$

$$B_{xt} = \sum_{i=1}^{n} B_x \ (i) \tag{14}$$

$$B_{yt} = \sum_{i=1}^{n} B_y \ (i) \tag{15}$$

$$B_{zt} = \sum_{i=1}^{n} B_z \ (i) \tag{16}$$

where, B_{xt} the summation of X axis magnetic field components, B_{yt} the summation of Y axis magnetic field components, and B_{zt} the summation of Z axis magnetic field components

$$B_t = B_{x_t}.\vec{a}_x + B_{y_t}.\vec{a}_y + B_{z_t}.\vec{a}_z \tag{17}$$

$$|B_t| = \sqrt{B^2_{x_t} + B^2_{y_t} + B^2_{z_t}} \tag{18}$$

Where, $\vec{a}_x$ Unit vector in X-direction, $\vec{a}_y$ Unit vector in Y-direction, and $\vec{a}_z$ Unit vector in Z-direction.
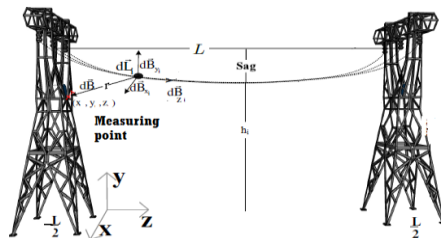

Figure 3. Application of Biot-Savart law in three dimensions

4. Results and Discussion

The phase-conductor currents are defined by a balanced direct-sequence three-phase set of 50 Hz sinusoidal currents. The direction of current is assumed to be along z-axis, which is pointing toward the observer. Magnetic field values are calculated based on sending end CT measured current, in which magnetic field values calculated at 17m, point P, above the ground to give the same values as directly measured based on non contact magnetoresistance sensor installed at the middle of the tower at point P under the tower M1 at sending end, closed to CT,
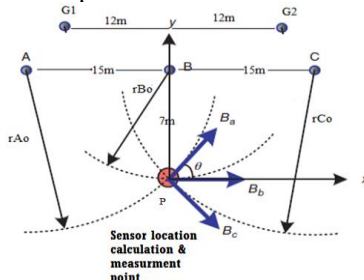

Figure 4. Magnetic field distribution at mid-point under the center phase
and under the tower M1 (point P)

as shown in figure 4. Measured currents from optic fiber CT placed at substation entrance, sending end, are transmitted to a data-processing center where Matlab software analysis, then the transient magnetic field from each line and resultant were calculated at point P as shown in figure 4.i.e. Ba, Bb, Bc, Bg1, Bg2, Bt. Figure 4 shows the magnetic field distribution at mid-point under the center phase and under the tower M1 (point P). M1 tower considered at sending end, which very closed to substation entrance CT.

A. Magnetic Field under Normal Condition

Figure 5 (a) shows the time variation of the calculated magnetic field and its components, at mid-point under the center phase and under the tower M1 (point P). It is noticed that, the magnetic field of the full load capacity reach to 18 µT. It's clear the waveform of the magnetic field is constant and stable.

Figure 5 (b) shows the computed magnetic field, Bt, Ba, Bb, and Bc at a different distances away from the center phase. it is noticed that the magnetic field at point P, under the center phase, reach to 18 µT, Phase B sharing with large ratio 16 µT, and the same magnetic field from phase A and C, 9.9 µT,.
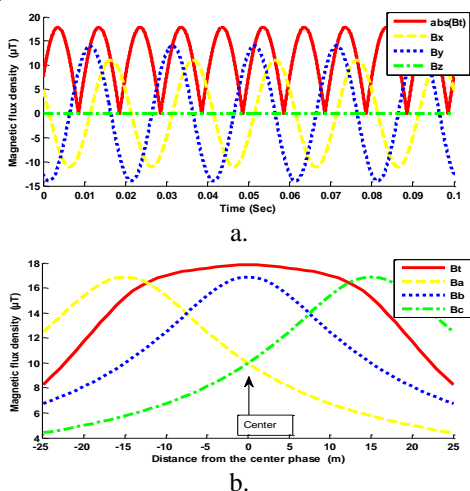

a.

b.

Figure 5. Under normal condition (a) Varying time magnetic field at (point P), (b) Total and individual phases field comparison at different distances from the center phase.

B. Magnetic Field under Abnormal Conditions

In this section, the effects of various types of faults were analyzed such as: single phase to ground fault, phase to phase fault, and three phase to ground fault, also direct lightning strokes, and flashover on the magnetic fields. The fault is cleared after the time that is taken by the protection device. The total fault clearing time equals 52 msec of the protection device [26, 34].

B.1. Single phase to ground fault

Figure 6 shows the calculated magnetic field and its components, during the single phase (A) to ground fault, at (point P). It is seen that from figure 6 (a) the maximum value of magnetic field equal 135.6 µT. also Bt in comparable with Ba, Bb, and Bc at a different distances away from the center phase. It is noticed that phase A, B, and C sharing with 126.6 µT (highest value), 17 µT, and 9.9 µT, respectively. Also the high overshot under phase A. It is noticed that, when single line (A) to ground fault occur, magnetic field for the faulted phase is higher compared with the healthy phase.
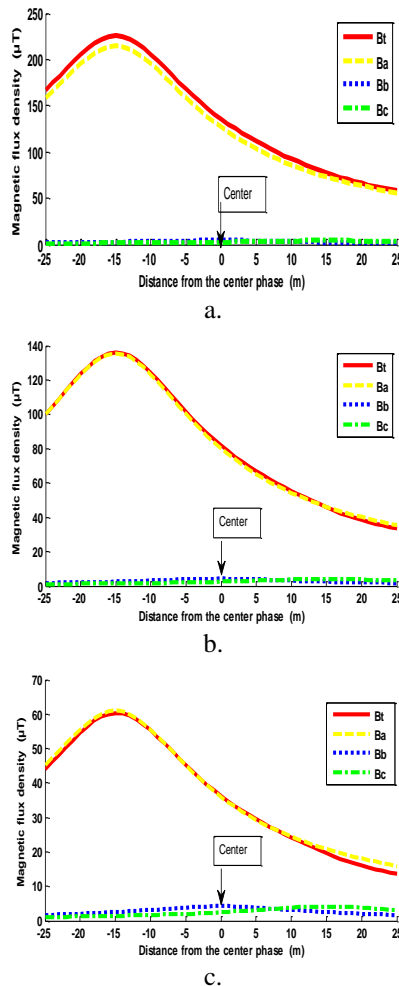

a.

b.

c.

Figure 6. Total and individual phase's field comparison at different distances from the center phase under phase A to ground fault (a) at 0 Ω fault resistance, (a) at 10 Ω fault resistance, and (b) at 30 Ω fault resistance

Figures 6 (b, c) show the magnetic field densities in case of fault resistance taken into account, 10 Ω, 30 Ω fault resistance respectively. It is noticed that the fault resistances have no

effect on accuracy of obtained results, i.e. the magnetic field for the faulted phase is higher compared with the healthy phase.

B.2. Three phase to ground fault

Figure 7 shows that the magnetic field, during the three phase to ground fault, at point P, under the center phase, reach to 308 µT, Phase A, B, and C sharing with 143 µT, 397 µT (highest value), and 97 µT, respectively.

It is noticed that, when three phase to ground fault occur, all the three phases magnetic field are higher than during its values comparing to normal condition.
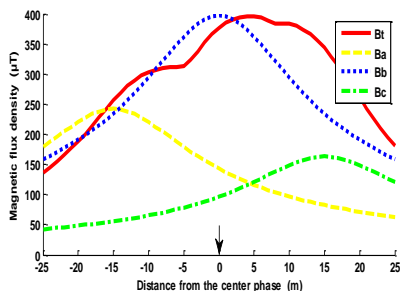

Figure 7. Total and individual phases field comparison at different distances from the center phase Under three phase to ground fault.

B.3. Phase to phase fault

Line-to-line fault, caused by ionization of air, or when lines come into physical contact. Figure 8 shows that the magnetic field, during the phase to phase fault at point P, under the center phase, reach to 235 µT, Phase A, B, and C sharing with 102 µT, 288 µT (highest value), and 9.8 µT, respectively.

It is shown that, when line to line fault occur, the magnetic field for the faulted phases is higher compared with the healthy phases, where the phase A and phase B magnetic field is much higher than phase C magnetic field.
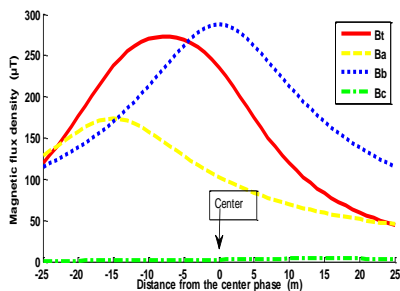
Figure 8. Total and individual phases field comparison at different distances from the center phase Under line A to line B fault.

C. Magnetic Field under Lightning Strokes

A current function model called Heidler is widely used to model a lightning current [16, 27, 28]. Eq. (19) represents the lightning current. A 400 Ω lightning path resistance was connected shunt to the simulated natural lightning.

$$i(t) = I_o \frac{(t/\tau_1)^2}{[(t/\tau_1)^2 + 1]} e^{-t/\tau_2} \tag{19}$$

where I_0: the peak of current, τ_1, τ_2 : time constants of current rising and dropping

### C.1. In case of direct lightning strokes

With effective shielding, it is possible to minimize direct strokes to the phase conductors, but this does not necessarily mean that the line will have satisfactory lightning performance. A shielding failure or a stroke to the conductor is essentially a single-phase. The lightning impulse is assumed to have (100 kA, 1/50 µs), and channel resistance equals 1 MΩ [29].

Figure 9 (a) shows the computed magnetic field, Bt, Ba, Bb, and Bc at a different distances away from the center phase, during the lightning strokes.

The result show that in case lightning hit phase (A), Bt reach to 537 µT, Phase A, B, and C sharing with 540 µT (large ratio), 16 µT, and 9.9 µT, respectively, as shown in figure 9 (a). It is observed, when lightning occur magnetic field for the struck phase conductor is higher compared with the non struck phase conductor.

Also figure 9 shows the Bt in comparable with Ba, Bb, and Bc at a different distances away from the center phase at 50kA-1/50 µs lightning stroke, as shown in figure 9 (b), and at 20kA-1/50 µs lightning stroke, as shown in figure 9 (c). It is seen that the lightning peak have no effect on accuracy of fault location and identification, i.e. the magnetic field for the lightning stroke phase is higher compared with the healthy phase.
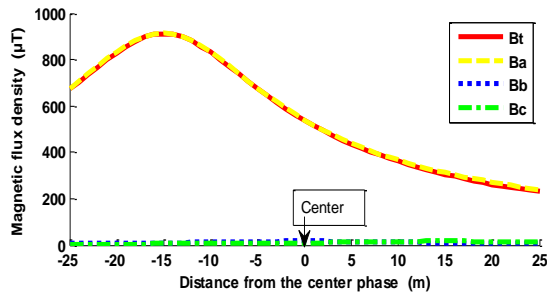
a.
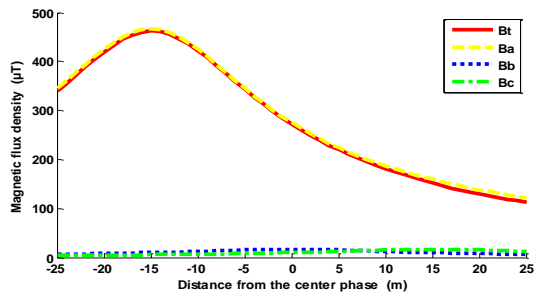
b.
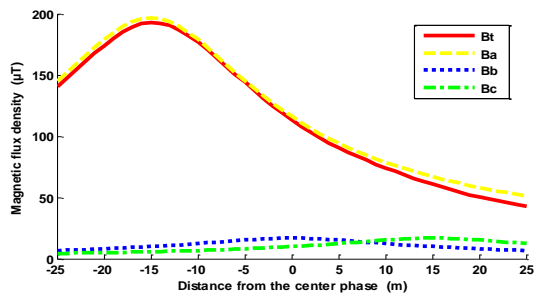
c.

Figure 9. Total and individual phase's field under lightning struck phase A (a) at 100kA-1/50 µs, (b) at 50kA-1/50 µs (c) at 20kA-1/50 µs

C.2. In case of insulator flash over

The lightning impulse is assumed to have (100 kA, 1/50 µs) [15, 27], and hit G1 or G2, and causes phase insulation flash over

Figure 10 shows the computed magnetic field, Bt, Ba, Bb, Bc, Bg1, and Bg2 at a different distances away from the center phase under indirect lightning strokes.

The result show that in case lightning hit ground wire G1 near phase (A), Bt reach to **470** µT, Phase A, B, C, G1, and G2 sharing with **893** µT (large value), **17** µT, **17** µT, 5.6 µT, and 5.6 µT, respectively, as shown in figure 10 (a). Also, in case lightning hit ground wire G2 near phase (C), Bt reach to 515 µT, Phase A, B, C, G1, and G2 sharing with 17 µT, 17 µT, 852 µT(large value), 276 µT, and 276 µT, respectively, as shown in figure 10 (b).
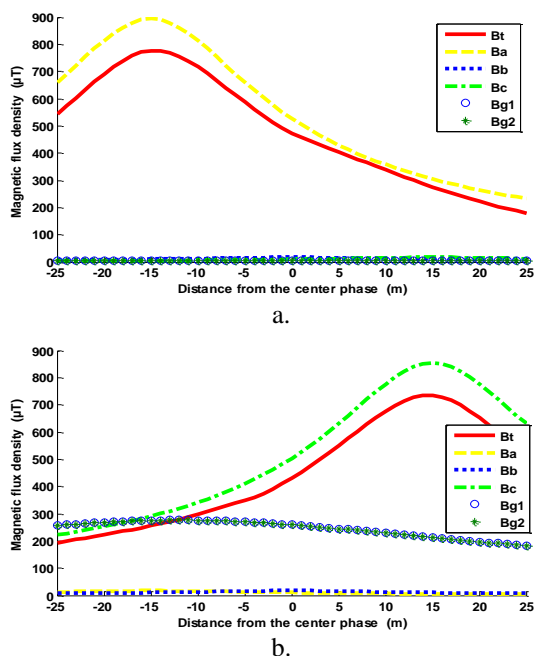

a.

b.

Figure 10. Magnetic field at (point P) under insulator flash over, Total and individual phases field comparison at different distances from the center phase. (a) lightning on G1, (b) lightning on G2

D. Scheme for fault and, lightning strokes detection, Classification and Location
a. Faults and, lightning strokes detection and classification scheme

Figure 11 shows the proposed scheme for fault detection and classification.

The proposed scheme is based on measured currents from CT at sending end under normal and abnormal conditions. Then data are transmitted to a data-processing center where analysis software such as Matlab software, in which magnetic field values as resultant magnetic field Bt, magnetic field from each phase conductor Ba, Bb, Bc, Bg1, and Bg2 calculated at point 17m above the ground level by using eqs. 3 to 18 stated above.

These calculated values the same as the measured values from only non contact Magnetoresistance magnetic sensor placed at tower M1, closed to CT, at point P (17m above the ground level). 3-axis Magnetoresistance sensor is a relatively newer generation of solid state magnetic sensors, the sensitivity can reach 1 picoTesla[30],vector sensor for magnetic field[31],small-size (sensor chip size around 3mm × 3 mm), good temperature tolerance, low power consumption (around 10 mW) which can be powered up by solar panel or electromagnetic power harvesting[26, 32], and wide operating frequency from DC to several MHz[33].

start

System Simulated using ATP-EMTP

Magnetic field calculated at sending end Bt, Ba, Bb, Bc, Bg1, and Bg2, and then data processed using Matlab

Fault detection stage

Bt >18 ±5% µT?

No → No Fault

Yes

Bg1>0?

No — Faults

Yes → Ba==Bb ==Bc

Yes → indirect lightning on G1 or G2 without flash over on phase s insulation string

Yes

Ba>Bc?

Yes → lightning on G1 cause flash over on phase A insulation string

No → lightning on G2 cause flash over on phase C insulation string

Fault classification stage

end

fault classification stage

(Ba>Bb) &&(Bb>Bc) — Yes → ('Single line (A) to ground fault or Lightning on phase A')

No

(Bb>Ba) &&(Ba==Bc) — Yes → ('Single line (B) to ground fault or Lightning on phase B')

No

(Bc>Bb) &&(Bb>Ba) — Yes → ('Single line (C) to ground fault or Lightning on phase C')

No

(Bb>Ba) &&(Ba>Bc) — Yes → ('Three phase fault')

No

(Bb>Ba) &&(Ba>Bc) && (Bc<=9.9) — Yes → ('Double line (AB) fault')

No

(Bc>Ba) &&(Ba>Bb) — Yes → ('Double line (AC) fault')

No

(Bb>Bc) &&(Bc>Ba)&&(Ba<=9.9) — Yes → ('Double line (BC) fault')
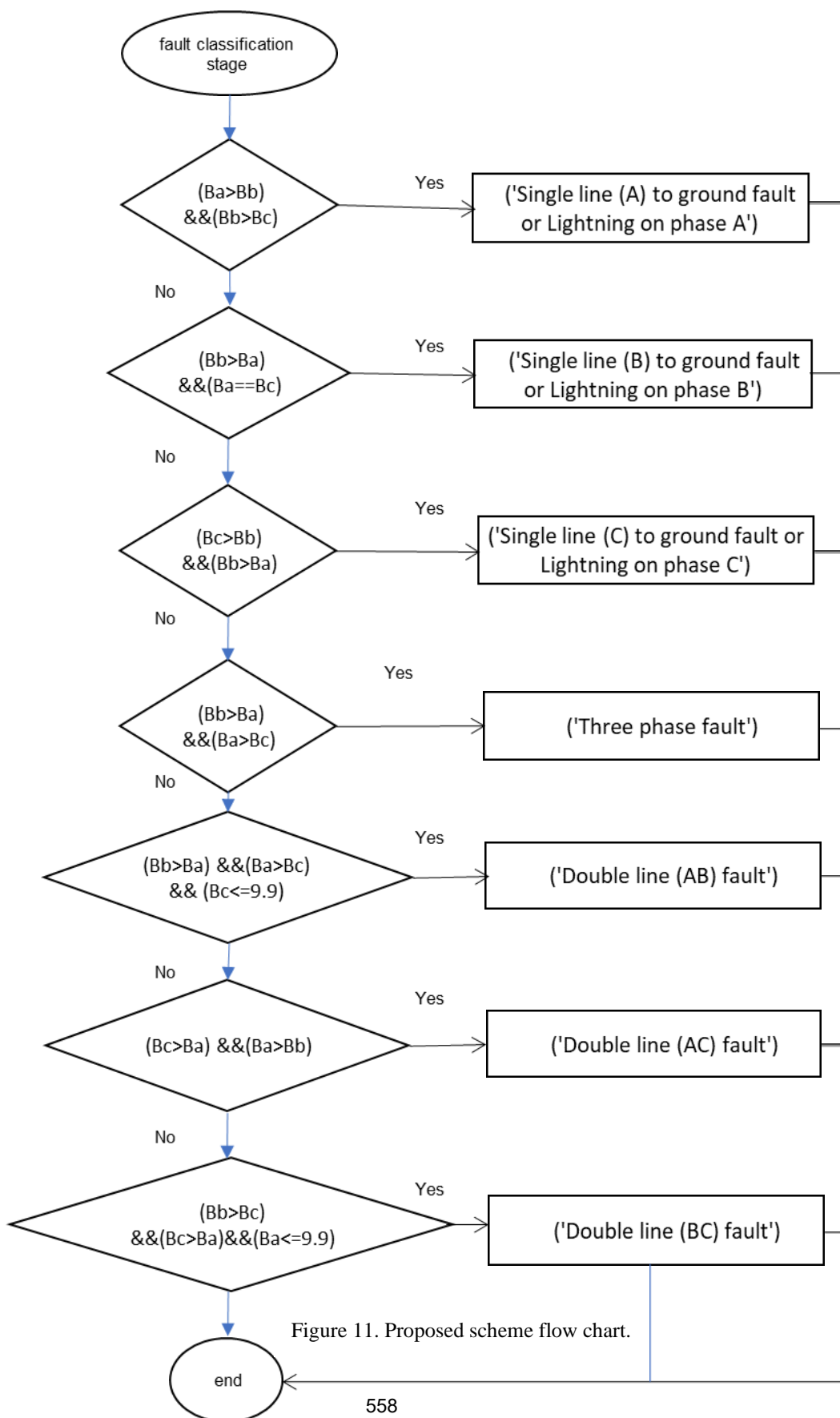
end

Figure 11. Proposed scheme flow chart.

Based on calculated or measured resultant transient magnetic field and each phases field it's clear that.

- The fault detection scheme was depend on comparing normal and abnormal resultant magnetic field. Table 1 shows magnetic field comparisons under different conditions. It's clear that the calculated transient magnetic field under abnormal conditions is greater than normal magnetic field, claim a fault. Where normal Bt is a predetermined threshold, and Bt=18 µT as stated in section 4.1 previously. And by assumption ±5% tolerance considering loading variation.

  Finally, fault detected in case of Bt above 18 ±5% µT.

- The fault classification scheme is based on not only Bt but also comparing calculated magnetic field from individual phase conductor Ba, Bb, Bc, Bg1, Bg2 under normal operation and abnormal condition, at mid-point under the center phase. Table 1 clear that for each abnormal condition has a unique relation between individual phases magnetic field. For example, in case single line (A) to ground fault, the Ba is greater than Bb and Bb is also greater than Bc. Finally, fault classified by a unique relation between phases transient magnetic fields.

<div align="center">Table 1 Analysis summary</div>

µT	Normal	three phase to ground	phase A to ground	phase B to ground	phase C to ground	phase A to B	phase A to C	phase B to C	direct lightning on A	direct lightning on B	direct lightning on C	indirect lightning on	indirect lightning on	flash over due to G1	flash over due to G2
		Abnormal conditions (Faults)													
(Bt)	18	308	135	355	207	235	272	295	537	893	517	34	34	470	515
Ba	16	143	165	9.9	9.9	102	166	9.9	540	18	18	16	16	893	17
Bb	9.9	397	17	355	17	288	17	367	16	890	16	16	16	17	17
Bc	9.9	97	9.9	9.9	82	9.9	107	76	9.9	9.9	525	16	16	17	852
Bg1	0	0	0	0	0	0	0	0	0	0	0	5.4	5.4	5.6	276
Bg2	0	0	0	0	0	0	0	0	0	0	0	5.4	5.4	5.6	276

b. Fault Location scheme

Figure 12 show the fault location scheme is based on dividing line length into sections each section contain, 3 tower, only one non contact magnetic field sensor installed at midpoint of tower, at one tower in section.

Then, magnetic field measurements under normal and abnormal condition at each section, a tower-mounted sensor require a conditioning circuitry with appropriate gain, microcontroller handling instrumentation chain and data communication link between the tower and the substation CT. the measured resultant magnetic field, at mid-point under the center phase and under the tower height, at selected towers along the transmission line was transmitted to a data-processing center where analysis software such as Matlab software. Finally, measured data compared with magnetic field calculated from substation entrance CT under different conditions. It's clear that the less ratio of (Bt measured using sensor at towers/ Bt calculated using CT at substation entrance) arrowed to the non faulted section.

The first jumping to high ratio after low ratio, indicates fault location section. Once the place of the faulted section is known, it is relatively easy for the line inspector to locate the specific point of the fault within the section.

For example, three phase fault to ground near M9 as shown in figure 13. To find optimum fault location adjacent to M9 by using Eq.(20) deduced from figure 14 by utilizing eq.3 the magnetic field caused by the right section of current is $B = -\dfrac{\mu_0 i}{4\pi a} * \cos\alpha_f$ .Therefore, the ratio of the measured magnetic field beside the fault point to the other measured magnetic field is: $\dfrac{1-\cos\alpha_f}{2}$ [11].

$$l = \frac{a}{tan(180 - cos^{-1}(1 - 2*\frac{Bt(measured)}{Bt(calculated)}))} \tag{20}$$

where, l is length from high ratio sensor, and (a) is vertical position of sensor.

5. Conclusion

In this paper, Egyptian Bassous-Cairo West 500-kV transmission line single circuit is modelled in ATP/EMTP. The transient magnetic field generated during the different faults, single line to ground, three phase, line to line fault, direct lightning strokes, and flash over were analyzed.

This paper presents a novel approach for fault detection, and classification scheme is based on calculating resultant magnetic field Bt, magnetic field from each conductor Ba, Bb, Bc, Bg1, Bg2 under normal operation and abnormal condition (which has unique behaviour), at mid-point under the center phase and under the tower, utilizing only fiber optic CT at substation entrance,. The high ratio of (Bt measured/ Bt calculated) indicate faulted section.

As seen from the simulation results, the fault resistances have no effect on accuracy of fault identification location. Accuracy of lightning stroke identification location was not depending on lightning stroke peak.

Finally, utilizing only fiber optic CT at substation entrance approach can accurately detect and identify the faults types. Also link between sensors at line section and CT at substation give good search for faults location.

List of Abbreviations:

3D: Three Dimensions, CT: Current Transformer, ATP-EMTP: Alternative Transients Program-Electro Magnetic Transients   Program.SA: Surge Arrester,OHTL: Over Head Transmission Line,GIS: Gas Insulated Substation, G.W: Ground Wire, LCC JMarti: Line Cable Conductor jose Marti., ρ :Soil Resistivity., εr: Relative Permittivity, μr:Relative Permeability, Vfo: Flashover Voltage, M1 to M18: Tower Name, Bt: magnetic flux density (Total), Magnetic field, Bx:Magnetic field component in X direction, By:Magnetic field component in Y direction, Bz:Magnetic field component in Z direction, Ba:Magnetic field from phase A, Bb:Magnetic field from phase B, Bc:Magnetic field from phase C, Bg1:Magnetic field from phase G1, Bg2:Magnetic field from phase G2.
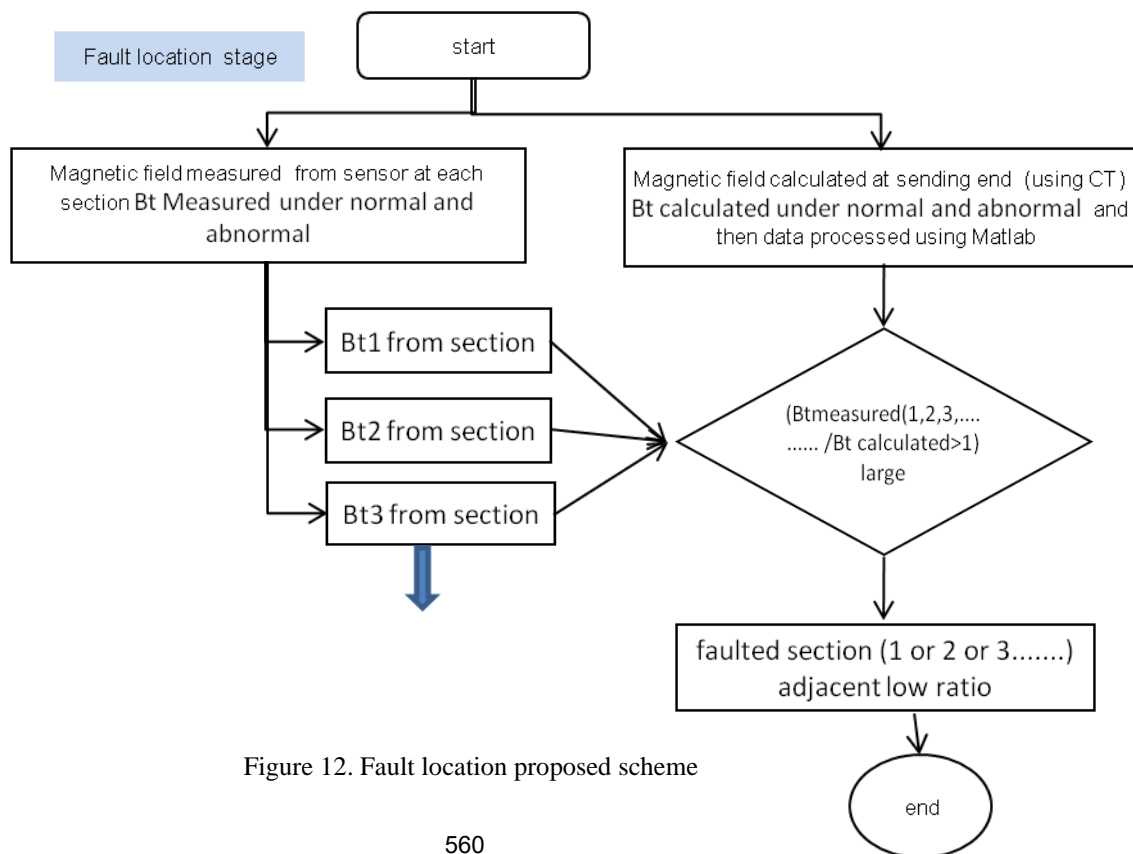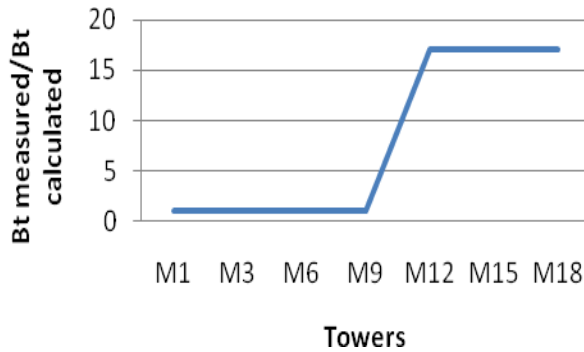
Figure 12. Fault location proposed scheme

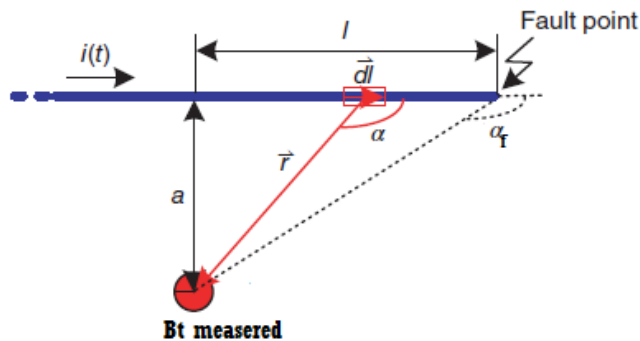Figure 13. Resultant magnetic field ratio comparisons at different towers

Figure 14. Fault distance from sensor calculation.

6. References

[1] Parmar, S.: ' Fault Location Algorithms for Electrical Power Transmission Lines', *Msc thesis*, Delft University of Technolog, 2015

[2] Liao, Yuan, Mladen Kezunovic.: 'Optimal estimate of transmission line fault location considering measurement errors', *IEEE Transactions on Power Delivery*., 2007, 22, (3), pp. 1335-1341

[3] Bouthiba, Tahar.: 'Fault location in EHV transmission lines using artificial neural networks', *International Journal of Applied mathematics and computer science*, 2004, 14, pp. 69-78

[4] Mohd Wazir Mustafa: 'Power System Analysis', Second edition, 2009

[5] M.Mirzaei, M.Z. A Ab Kadir, E.Moazami, H.Hizam.:'Review of fault location methods for distribution power system', *Australian Journal of Basic and Applied Sciences*., 2009, 3, (3), pp. 2670-2676

[6] Das, R., M. S. Sachdev, T. S. Sidhu.: 'A fault locator for radial subtransmission and distribution lines', Power Engineering Society Summer Meeting, IEEE., 2000, 1

[7] Myeon-Song Choi, Seung-Jae Lee., et al.:'A new fault location algorithm using direct circuit analysis for distribution systems', *IEEE Transactions on Power Delivery*, 2004, 19, (1), pp. 35-41

[8] Raval, Pranav D.: 'ANN based classification and location of faults in EHV transmission line', *International multiconference of engineers and computer scientists*, Hongkong, 2008

[9] Jain, A. Thoke, A.S. Patel, R.N.: 'Double Circuit Transmission Line Fault Distance Location Using Artificial Neural Network', *World Congress on Nature & Biologically Inspired Computing*., 2009, pp. 13-18

[10] IEEE Guide for Determining Fault Location on AC Transmission and Distribution Lines, IEEE Std C37.114-2004, 2005, Power Syst. Relay. Comm., E-ISBN: 0-7381-4654-4.

[11] Huang, Q., Zhen, W., et al.: 'A novel approach for fault location of overhead transmission line with noncontact magnetic-field measurement', *IEEE Transactions on Power Delivery*., 2012, 27, (3), pp. 1186-1195

[12] Li, Yajie, Xiaoli Meng, Xiaohui Song.: 'Application of signal processing and analysis in detecting single line-to-ground (SLG) fault location in high-impedance grounded distribution network', *IET Generation, Transmission & Distribution*., 2016, 10, (2), pp. 382-389

[13] Saini, Makmur, et al. 'Algorithm for Fault Location and Classification on Parallel Transmission Line using Wavelet based on Clarke's Transformation', *International Journal of Electrical and Computer Engineering (IJECE)*, 2018, 8, (2), pp. 699-710

[14] http://www.atpdraw.net/, 2015.

[15] ANSI/IEEE Std 80-1986' Ac Substation Grounding'

[16] A.said.: 'Analysis of 500 kV OHTL polluted insulator string behavior during lightning strokes", *International Journal of Electrical Power & Energy Systems*, 2018, 95, pp. 405-416

[17] Abdelrahman Said Ghoniem.: 'Effective Elimination Factors to the Generated Lightning Flashover in High Voltage Transmission Network', *International Journal on Electrical Engineering and Informatics*, 2017, 3, pp. 455-468

[18] J. Marti.: 'Accurate Modeling of Frequency Dependent Transmission Lines in Electromagnetic Transients Simulation', *IEEE Transactions on Power Apparatus and Systems*, PAS-101, 1982, 1, pp. 147–157

[19] Pinceti P, Giannettoni M.: 'A simplified model for zinc oxide surge arresters', *IEEE Transaction on Power Delivery*, 1999, 14, (2), pp. 393–398

[20] Adel Z. El Dein.:'The Effects of the Span Configurations and Conductor Sag on the Magnetic-Field Distribution under Overhead Transmission Lines', *Journal of Physics*., 2012, 1, (2), pp. 11–23

[21] Khawaja, Arsalan Habib, Qi Huang.: 'Estimating Sag and Wind-Induced Motion of Overhead Power Lines with Current and Magnetic-Flux Density Measurements', *IEEE Transactions on Instrumentation and Measurement*., 2017, 66, (5), pp. 897-909.

[22] R. D. Begamudre.:'Extra High Voltage AC. Transmission Engineering', NJ: *Wiley Eastern, third edition Hoboken*, ch. 7, 2006, pp. 172–205

[23] Abhishek Gupta.: 'A Study on High Voltage AC Power Transmission Line Electric and Magnetic Field Coupling with Nearby Metallic Pipelines', *M.Sc. Thesis*, Indian Institute of Science, 2006.

[24] Ossama E. Gouda, Adel Z. El Dein, M.A.El-Gabalawy.: ' Effect of electromagnetic field of overhead transmission lines on the metallic gas pipe-lines', *Electrical Power Systems Research, Elsevier* ., 2013, 103, pp. 129–136

[25] Adel Z. El Dein.: ' Mitigation of Magnetic Field under Egyptian 500kv Overhead Transmission Line ', *World Congress on Engineering* 2010, 2, London, U.K., June 30 – July 2

[26] Khawaja, Arsalan Habib, Qi Huang.: 'Characteristic estimation of high voltage transmission line conductors with simultaneous magnetic field and current measurements', *Instrumentation and Measurement Technology Conference Proceedings (I2MTC)*, 2016

[27] Ossama E. Gouda, Adel Z. El Dein, Ghada M. Amer.: 'Parameters Affecting the Back Flashover across the Overhead Transmission Line Insulator Caused by Lightning', *14th International Middle East Power Systems Conference (MEPCON'10)*, Cairo University, 2010, 111

[28] Taheri, Sh, A. Gholami, M. Mirzaei.: 'Study on the behavior of polluted insulators under lightning impulse stress', *Electric Power Components and Systems*, 2009, 37, (12), pp. 1321-1333

[29] J. Rohan Lucas.: 'High Voltage Engineering', Second Edition, Book, Chapter 3, Sri Lanka, 2001, pp. 34 – 43

[30] W. E. Jr., P. Pong, J. Unguris., et al.: 'Critical challenges for picotesla magnetic-tunnel-junction sensors', *Sensors and Actuators A: Physical*, 2009, 155, (2), pp. 217–225

[31] P. P. Freitas, R. Ferreira., et al.: 'Magnetoresistive sensors', *Journal of Physics: Condensed Matter*., 2007, 19, (16), pp. 165-221

[32] Zangl, Hubert, Thomas Bretterklieber, Georg Brasseur.:'A feasibility study on autonomous online condition monitoring of high-voltage overhead power lines', *IEEE Transactions on Instrumentation and Measurement*., 2009, 58, (5), pp. 1789-1796.

[33] A. B. E. Dallago, P. Malcovati, et al.: 'A fluxgate magnetic sensor: From PCB to micro-integrated technology', *IEEE Transactions on Instrumentation and Measurement*., 2007, 56, (1), pp. 25–31

[34] Abdel-Gawad, Nagat MK, Adel Z. El Dein, and Mohamed Magdy. "Magnetic Field Calculation under Normal and Abnormal Conditions of Overhead Transmission Lines." *TELKOMNIKA Indonesian J. Electrical Eng*. 12. May (5) (2014): 3381-3391.

Abdelrahman Said Ghoniem was born in Cairo, Egypt, on March 9, 1987. He received the B.Sc. degree in Electrical Power and Machines with honor in 2009, the M.Sc. degree in High Voltage Engineering in 2013, and the Ph.D. degree in High Voltage Engineering in 2016, all from Electrical Power and Machines Department, Faculty of Engineering at Shoubra, Benha University, Cairo, Egypt. He is currently a Lecturer with the Electrical Engineering department, Faculty of Engineering at Shoubra, Benha university. His research activity includes: Transient Phenomenon in Power Networks, Artificial intelligent in power system, Renewable energy.